Inorg. Chem. **2003**, *42*, 3492–3500

Antiferromagnetic Three-Dimensional Order Induced by Carboxylate Bridges in a Two-Dimensional Network of $[Cu_3(dcp)_2(H_2O)_4]$ Trimers

Philippa King,[†] Rodolphe Clérac,*[,‡] Christopher E. Anson,[†] Claude Coulon,[‡] and Annie K. Powell*[,†]

Institut für Anorganische Chemie der Universität Karlsruhe, Engesserstr. Geb. 30.45, D-76128 Karlsruhe, Germany, and Centre de Recherche Paul Pascal, CNRS UPR 8641, Avenue Dr. A. Schweitzer, 33600 Pessac, France

Received November 14, 2002

A new Cu(II) complex, $[Cu_3(dcp)_2(H_2O)_4]_n$, with the ligand 3,5-pyrazoledicarboxylic acid monohydrate (H_3dcp) has been prepared by hydrothermal synthesis, and it crystallizes in the monoclinic space group $P2_1/c$ with $a = 11.633(2)$ Å, $b = 9.6005(14)$ Å, $c = 6.9230(17)$ Å, $\beta = 106.01(2)°$, and $Z = 2$. In the solid state structure of $[Cu_3(dcp)_2(H_2O)_4]_n$, trinuclear $\{Cu_3(dcp)_2(H_2O)_4\}$ repeating units in which two dcp^{3-} ligands chelate the three Cu(II) ions with the central Cu(II) ion, Cu(1) (on an inversion center), link to form infinite 2D sheets via syn–anti equatorial–equatorial carboxylate bridges between Cu(2) atoms in adjacent trimers. These layers are further linked by syn–anti axial–equatorial carboxylate bridging between Cu(1) atoms in adjacent sheets resulting in the formation of a crystallographic 3D network. A detailed analysis of the magnetic properties of $[Cu_3(dcp)_2(H_2O)_4]_n$ reveals that the dcp^{3-} ligand acts to link Cu(II) centers in three different ways with coupling constants orders of magnitude apart in value. In the high temperature region above 50 K, the dominant interaction is strongly antiferromagnetic ($J/k_B = -32$ K) within the trimer units mediated by the pyrazolate bridges. Below 20 K, the trimer motif can be modeled as an $S = {}^1/_2$ unit. These units are coupled to their neighbors by a ferromagnetic interaction mediated by the syn–anti equatorial–equatorial carboxylate bridge. This interaction has been estimated at $J_{2D}/k_B = +2.8$ K on the basis of a 2D square lattice Heisenberg model. Finally, below 3.2 K a weak antiferromagnetic coupling ($J_{3D}/k_B = -0.1$ K) which is mediated by the *syn-anti axial–equatorial* carboxylate bridges between the 2D layers becomes relevant to describe the magnetic (T, H) phase diagram of this material.

Introduction

Recent years have witnessed an explosion of interest in the synthesis of molecular-based magnetic solids.[1] An important concept here is the use of molecular building blocks to create systems of varying dimensionalities, ranging from zero-dimensional, essentially molecular or nanoscale objects, to extended three-dimensional networks. In terms of creating new magnetic solids, zero-dimensional systems are of interest when they display the so-called property of "single molecule magnetism"; one-dimensional systems are important in understanding the properties of chains, but will not display long-range order, while the two- and three-dimensional systems may show long-range order and thus could find applications as new molecular-based magnetic materials. In all cases, the magnetic bricks display properties whose origins lie in the molecular nature of the system. In theory, this makes it possible to direct the properties of the magnetic brick by favoring certain molecular motifs, for example, by connecting two paramagnetic centers in such a way as to favor magnetic exchange which might induce either parallel or antiparallel spin pairing. Previous work by researchers such as Kahn has shown that organizing ferromagnetic, spin parallel, arrangements in extended 2D or 3D systems is difficult for such molecular-based systems.[2,3] In fact, it is much easier to create spin lattices where antiferromagnetic, spin antiparallel, interactions predominate. This does not preclude the formation of magnets since a

* To whom correspondence should be addressed. E-mail: powell@achpc50.chemie.uni-karlsruhe.de (A.K.P.); clerac@crpp.u-bordeaux.fr (R.C.). Phone: +49 721 608 2135 (A.K.P.); +33 5 56 84 56 50 (R.C.). Fax: +49 721 608 8142 (A.K.P); +33 5 56 84 56 00 (R.C.).

[†] Institut für Anorganische Chemie der Universität Karlsruhe.

[‡] Centre de Recherche Paul Pascal, CNRS.

(1) *Polyhedron* **2000**, *20* (11−14), entire issue.

(2) Larionova, J.; Clérac, R.; Sanchiz, J.; Kahn, O.; Golhen, S.; Ouahab, L. *J. Am. Chem. Soc.* **1998**, *120* (50), 13088−13095.

(3) Larionova, J.; Kahn, O.; Golhen, S.; Ouahab, L.; Clérac, R. *J. Am. Chem. Soc.* **1999**, *121* (14), 3349−3356.

10.1021/ic0261777 CCC: $25.00
Published on Web 05/09/2003

Scheme 1

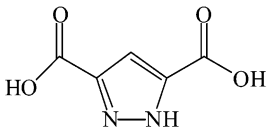

H_3dcp

remanent magnetization can be observed in ferrimagnetic or spin-canted antiferromagnetic phases which are special cases where antiferromagnetic interactions are present. Here we report the synthesis, characterization, and magnetic properties of $[Cu_3(dcp)_2(H_2O)_4]_n$ which has been hydrothermally produced and displays an antiferromagnetic ground state.

We have shown previously the utility of the hydrothermal synthetic method in creating molecular-based magnetic solids with relatively high spin densities and a range of magnetic properties.[4−6] This method has been used extensively for the production of zeolites[7] and is now proving to be an effective and simple technique for the synthesis of inorganic coordination compounds in crystalline form.[8−10] In this synthetic approach, the reduced viscosity of water at temperatures above 100 °C combined with autogenous pressure promotes solvent extraction of solids and crystal growth from solution. In addition, the use of relatively mild conditions allows complex organic molecules to remain stable and in turn promotes the self-assembly of new phases which under ambient conditions would not be kinetically favorable.[11,12] By using this approach, new structural motifs can be observed which would not be obtained by ambient synthesis. Furthermore, very densely packed compounds can be obtained using hydrothermal methods, or alternatively, by use of specific bases which act as templates, open packing systems can be synthesized as seen for zeolites.[7] Hydrothermal synthesis is a particularly effective synthetic technique for use with rigid ligands, such as in this case H_3dcp.[8,13]

The ligand H_3dcp (Scheme 1) has potential coordination sites involving both the nitrogen atoms of the pyrazole ring and all of the carboxylate oxygens. These multifunctional coordination sites are highly accessible to metal ions, and as such, H_3dcp can coordinate as a mono-, bi-, or tetradentate ligand and can act to link together metal centers through a number of bridging modes. A variety of coordination compounds containing transition, lanthanide and alkaline-earth metals have been synthesized and reported in the literature.[13−20] The $[Cu_3(dcp)_2(H_2O)_4]_n$ compound we report here is the first example where all six donors of the dcp^{3-} ligand are observed to coordinate to the metal centers.

Table 1. Crystal Data and Structure Refinement Summary for $[Cu_3(dcp)_2(H_2O)_4]_n$, **1**

empirical formula	$C_{10}H_{10}Cu_3N_4O_{12}$
fw	568.84
T/K	200(2)
cryst syst	monoclinic
space group	$P2_1/c$
a/Å	11.633(2)
b/Å	9.6005(14)
c/Å	6.9230(17)
β/deg	106.01(2)
V/Å^3	743.2(3)
Z	2
D (calcd)/g cm^{-3}	2.54
cryst size	0.17 × 0.11 × 0.06 mm^3
data measured	2963
indep reflns	1256
R_{int}	0.0599
obsd data ($I > 2\sigma(I)$)	1112
wR2	0.1627 (all data); 0.1554 (obsd)
R1	0.0557 (all data); 0.0503 (obsd)
GOF on F^2	1.125 (all data)

Experimental Section

Materials. All chemicals and solvents (purchased from Aldrich and Lancaster) used for synthesis were reagent grade and used without further purification.

Preparation of the Compound $[Cu_3(dcp)_2(H_2O)_4]_n$. A solution of $H_3dcp \cdot H_2O$ (0.070 g, 0.40 mmol) in H_2O (3.3 mL) and a solution of KOH (0.067 g, 1.20 mmol) in H_2O (3.3 mL) were added to an aqueous solution (3.3 mL) of $Cu(NO_3)_2 \cdot 3H_2O$ (0.097 g, 0.40 mmol) and stirred. The resultant blue solution was placed in a Teflon-lined autoclave with a capacity of 23 cm^3 which was then heated to 165 °C for 16 h. The autoclave was allowed to cool to room temperature over a period of approximately 16 h before it was opened. The blue crystals of $[Cu_3(dcp)_2(H_2O)_4]_n$ obtained by this hydrothermal synthesis were isolated by filtration and washed with water. Yield 0.082 g, 36.04%. Anal. Calcd for $C_{10}H_{10}Cu_3N_4O_{12}$: C, 21.11; H, 1.77; N, 9.85. Found: C, 21.07; H, 1.51; N, 9.64. IR (400−4000 cm^{-1}): 3455 (m/s, br), 3221 (m, br), 3160 (m, vsp), 2918 (m, br), 1631 (s, m/br), 1547 (s, sp), 1522 (s, sp), 1404 (s, sp), 1342 (s, sp), 1332 (s, sp), 1295 (s, sp), 1096 (vw, sp), 1067 (m, sp), 1019 (w, sp), 851 (m, sp), 787 (m, sp), 738 (m, m), 619 (m, m), 572 (w, sp), 470 (w, br).

Analytical Procedures. The infrared spectrum was measured using the KBr disk method on a Nicolet 4020 FT-IR spectrometer. Elemental analysis for C, H, and N was performed at the Inorganic Chemistry Department of the University of Karlsruhe.

X-ray Crystallography. Crystal data and final *R*-factors are summarized in Table 1. A blue crystal (thin plate) of dimensions

(4) Price, D. J.; Powell, A. K.; Wood, P. T. *J. Chem. Soc., Dalton Trans*. **2000**, 3566−3569.
(5) Price, D. J.; Tripp, S.; Powell, A. K.; Wood, P. T. *Chem. Eur. J*. **2001**, *7*, 200−208.
(6) Gutschke, S. O. H.; Price, D. J.; Powell, A. K.; Wood, P. T. *Inorg. Chem*. **2000**, *39*, 3705−3707.
(7) Barrer, R. M. *Hydrothermal Chemistry of Zeolites*; Academic Press: New York, 1982.
(8) Pan, L.; Frydel, T.; Sander, M. B.; Huang, X.; Li, J. *Inorg. Chem.* **2001**, *40*, 1271−1283 and references therein.
(9) Finn, R. C.; Lam, R.; Greedan, J. E.; Zubieta, J. *Inorg. Chem*. **2001**, *40*, 3745−3754.
(10) Rabenau, A. *Angew. Chem., Int. Ed. Engl.* **1985**, *24*, 1026−1040.
(11) Laudise, R. A. *Chem. Eng. News* **1987**, *65*, 30−43.
(12) Rao, C. N. R. *Materials Science and Engineering.* **1993**, *B18*, 1−21.
(13) Pan, L.; Ching, N.; Huang, X.; Li, J. *Chem. Eur. J.* **2001**, *7*, 4431−4437.
(14) Wenkin, M.; Devillers, M.; Tinant, B.; Declercq, J. *Inorg. Chim. Acta* **1997**, *258*, 113−118.
(15) Hahn, C. W.; Rasmussen, P. G.; Bayon, J. C. *Inorg. Chem.* **1992**, *31*, 1963−1965.
(16) Sanna, D.; Micera, G.; Buglyo, P.; Kiss, T.; Gajda, T.; Surdy, P. *Inorg. Chim. Acta* **1998**, *268*, 297−305.
(17) Sakagami, N.; Nakahanada, M.; Ino, K.; Hioki, A.; Kaizaki, S. *Inorg. Chem*. **1996**, *35*, 683−688.
(18) Nakahanada, M.; Ino, K.; Kaizaki, S. *J. Chem. Soc., Dalton Trans.* **1993**, 3681−3684.
(19) Wenkin, M.; Touillaux, R.; Devillers, M. *New J. Chem*. **1998**, 973−976.
(20) Sakagami-Yoshida, N.; Teramoto, M.; Hioki, A.; Fuyuhiro, A.; Kaizaki, S. *Inorg. Chem*. **2000**, *39*, 5717−5724.

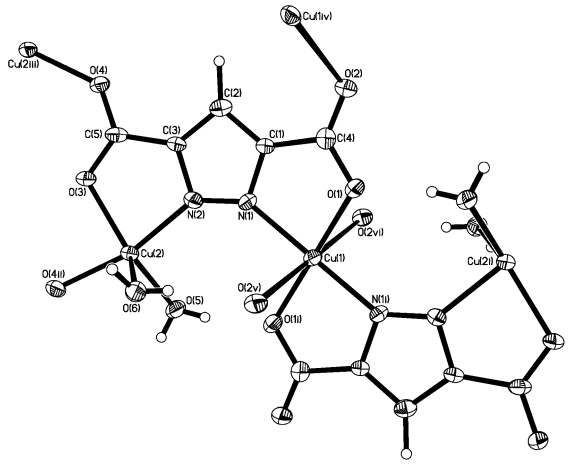

Figure 1. ORTEP drawing of the trinuclear $[Cu_3(dcp)_2(H_2O)_4]$ repeating unit in **1** (50% probability thermal ellipsoids). Symmetry codes for atoms of adjacent units: i $\{-x+1, -y+1, -z\}$; ii $\{-x+2, y+1/2, -z+1/2\}$; iii $\{-x+2, y-1/2, -z+1/2\}$; iv $\{-x+1, y-1/2, -z+1/2\}$; v $\{-x+1, y+1/2, -z+1/2\}$; vi $\{x, -y+1/2, z-1/2\}$.

$0.17 \times 0.11 \times 0.06$ mm^3 was mounted in oil on a Stoe IPDS area detector diffractometer equipped with graphite-monochromatized Mo Kα radiation ($\lambda = 0.71073$ Å) and cooled to 200 K using an Oxford Cryostream 600 temperature controller. A total of 2963 reflections were measured, of which 1256 were unique ($R_{int} = 0.0599$) and 1112 with $I > 2\sigma(I)$ were designated observed. Structure solution by direct methods and full-matrix refinement on F^2 (all data) were carried out using the SHELXTL software suite.[21] All non-H atoms were refined anisotropically. The coordinates of the water H atoms were refined (U fixed at $1.5U_{eq}$ of the respective O atom), while the aromatic H atom was placed in its calculated position. All crystals of **1** studied were found to exhibit a pseudomerohedric twinning, with the twin law corresponding to reflection in a plane perpendicular to the *c*-axis (corresponding to the plane of the infinite sheets, see later discussion). The primitive unit cell can be transformed to a C-centered cell that is close to orthorhombic, but R_{int} becomes over twice as high, and the structure could not be refined in any space group in this crystal system. However, a consequence of this pseudosymmetry is that each reciprocal lattice point for the primitive monoclinic unit cell is almost coincident with a point in the reciprocal lattice of the twin, so that the twinning could readily be handled with the command TWIN −1 0 −1 0 −1 0 0 0 1 2 in SHELXTL. The scale factor for the minor twin component refined to 0.32035 for the crystal used and allowed satisfactory refinement of the structure to final *R*-indices wR2 = 0.1627 (all data) and conventional R1 = 0.0503 (observed data).

Magnetic Measurements. The magnetic susceptibility measurements were obtained with the use of a Quantum Design SQUID MPMS-XL susceptometer. Measurements were performed on a polycrystalline sample of $[Cu_3(dcp)_2(H_2O)_4]_n$ (24.38 mg). Direct current (DC) measurements were collected from 1.8 to 320 K and from −50 to 50 kOe. Alternating current (AC) measurements were performed at various frequencies from 1 to 1500 Hz with an AC field amplitude of 3 Oe and with a static field applied ranging from 0 to 50 kOe. The magnetic data were corrected for the sample holder, and the diamagnetic contribution was calculated from Pascal's constants.[22] The electron paramagnetic resonance (EPR) was performed using polycrystalline samples at X-band on a Bruker ESP300E spectrometer at room temperature.

Table 2. Selected Bond Lengths [Å] and Angles [deg] for $[Cu_3(dcp)_2(H_2O)_4]_n$, **1**[a]

Cu(1)−O(1)	1.960(5)	N(1)−N(2)	1.333(8)
Cu(1)−N(1)	1.978(5)	N(1)−C(1)	1.351(9)
Cu(1)−O(2v)	2.673(6)	N(2)−C(3)	1.358(8)
Cu(2)−N(2)	1.973(5)	C(1)−C(2)	1.379(9)
Cu(2)−O(3)	2.042(5)	C(1)−C(4)	1.486(9)
Cu(2)−O(4ii)	1.955(4)	C(2)−C(3)	1.390(9)
Cu(2)−O(5)	1.956(6)	C(3)−C(5)	1.478(8)
Cu(2)−O(6)	2.230(6)	C(4)−O(2)	1.224(1)
		C(4)−O(1)	1.293(9)
		C(5)−O(4)	1.252(8)
		C(5)−O(3)	1.260(8)

O(1)−Cu(1)−O(1i)	180	O(3)−Cu(2)−O(6)	116.5(3)
N(1)−Cu(1)−N(1i)	180	O(5)−Cu(2)−O(6)	97.0(3)
O(2v)−Cu(1)−O(2vi)	180	Cu(2)−O(3)−C(5)	113.6(4)
O(1)−Cu(1)−N(1)	82.6(2)	N(1)−N(2)−Cu(2)	138.1(4)
O(1)−Cu(1)−N(1i)	97.4(2)	C(3)−N(2)−Cu(2)	112.4(4)
O(1)−Cu(1)−O(2v)	100.9(2)	C(5)−O(4)−Cu(2iii)	134.5(4)
O(1)−Cu(1)−O(2vi)	79.1(2)	N(2)−N(1)−C(1)	108.4(5)
N(1)−Cu(1)−O(2vi)	93.7(2)	N(1)−N(2)−C(3)	107.9(5)
N(1)−Cu(1)−O(2v)	86.3(2)	N(1)−C(1)−C(2)	110.2(6)
N(2)−N(1)−Cu(1)	140.2(4)	N(1)−C(1)−C(4)	116.1(6)
Cu(1)−O(1)−C(4)	115.6(4)	C(2)−C(1)−C(4)	133.5(7)
C(1)−N(1)−Cu(1)	111.0(4)	C(1)−C(2)−C(3)	103.6(6)
C(4)−O(2)−Cu(1iv)	119.5(5)	N(2)−C(3)−C(2)	109.8(5)
N(2)−Cu(2)−O(4ii)	165.8(2)	N(2)−C(3)−C(5)	115.6(5)
N(2)−Cu(2)−O(3)	81.7(2)	C(2)−C(3)−C(5)	134.3(6)
N(2)−Cu(2)−O(5)	96.5(2)	O(1)−C(4)−O(2)	125.1(6)
N(2)−Cu(2)−O(6)	89.2(3)	O(2)−C(4)−C(1)	121.4(7)
O(4ii)−Cu(2)−O(3)	84.7(2)	O(1)−C(4)−C(1)	113.5(6)
O(4ii)−Cu(2)−O(5)	97.0(2)	O(3)−C(5)−O(4)	125.8(6)
O(4ii)−Cu(2)−O(6)	93.5(2)	O(4)−C(5)−C(3)	117.8(6)
O(3)−Cu(2)−O(5)	146.3(3)	O(3)−C(5)−C(3)	116.2(6)

[a] Symmetry transformations used to generate equivalent atoms: i, $-x+1, -y+1, -z$; ii, $-x+2, y+1/2, -z+1/2$; iii, $-x+2, y-1/2, -z+1/2$; iv, $-x+1, y-1/2, -z+1/2$; v, $-x+1, y+1/2, -z+1/2$; vi, $x, -y+1/2, z-1/2$.

Results and Discussion

Synthesis. In order to isolate $[Cu_3(dcp)_2(H_2O)_4]_n$ (**1**), hydrothermal synthesis was employed. Previous publications have reported the synthesis of crystalline compounds, with the ligand H_3dcp, under ambient conditions.[14−20] In contrast, our work with Cu(II) has shown that reactions using these conditions generate mainly amorphous materials,[23] whereas, using hydrothermal synthesis, a range of crystalline complexes with several different structural types result.[8,13,24]

Structure Analysis. The basic trinuclear repeating unit in the title compound $[Cu_3(dcp)_2(H_2O)_4]_n$ (**1**) is shown in Figure 1. Selected bond lengths and angles are listed in Table 2.

The crystal structure of **1** consists of two-dimensional sheets of $[Cu_3(dcp)_2(H_2O)_4]$ trimers. The planar trinuclear units contain a six-coordinate and two five-coordinate Cu(II) ions chelated by two dcp^{3-} ligands, in which the intratrimer Cu(1)···Cu(2) distance is 4.356(1) Å. The central copper atom, Cu(1), lies on a crystallographic inversion

(21) Sheldrick, G. M. *SHELXTL 5.1*; Bruker AXS Inc.: Madison, WI, 1997. Neutral atom scattering factors, f' and f'', were taken from: *International Tables for Crystallography, Vol. C*; Wilson, A. J. C., Ed.; Kluwer Academic Publishers: Dordrecht, 1992; pp 500−502 (Table 6.1.1.4) and 219−222 (Table 4.2.6.8).

(22) *Theory and Applications of Molecular Paramagnetism*; Boudreaux, E. A., Mulay, L. N., Eds; John Wiley & Sons: New York, 1976.
(23) King, P. MSc Thesis, UEA, Norwich, 2000.
(24) King, P.; Powell, A. K. In progress.

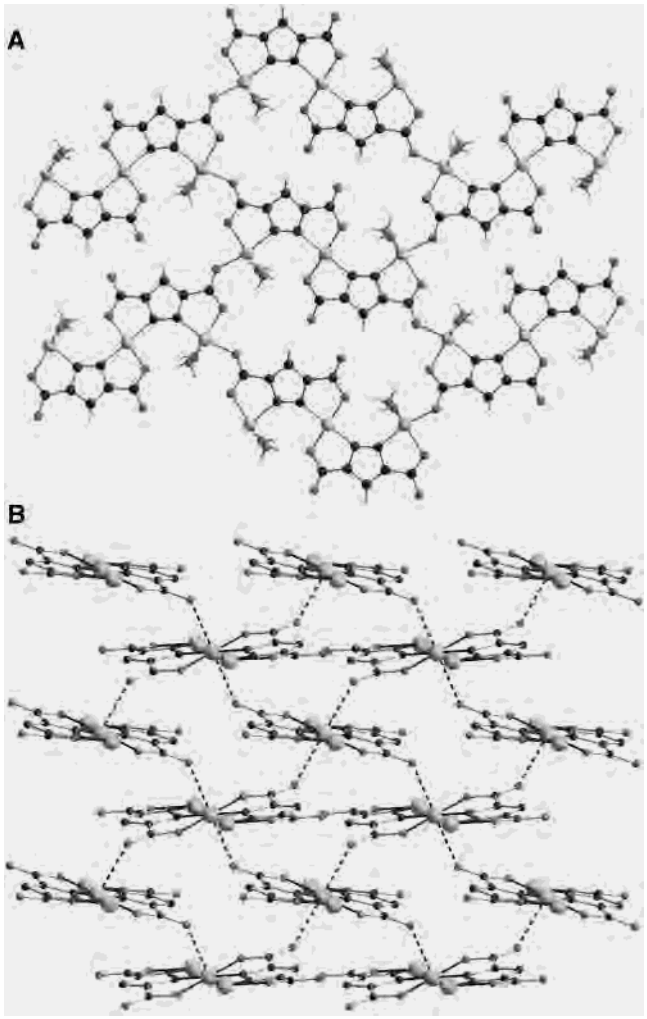

Figure 2. (A) Packing diagram of **1** showing the infinite sheets of the [Cu$_3$(dcp)$_2$(H$_2$O)$_4$] units (in the *(a,b)* plane). (B) The linkage of trinuclear units in adjacent sheets through nonplanar syn−anti carboxylate bridges (- - -) between Cu(1) centers in different sheets (aqua ligands and H-atoms omitted for clarity).

center. Syn−anti equatorial−equatorial carboxylate bridges between Cu(2) atoms in adjacent trimers link this basic repeating unit to form an infinite 2D plane (Figure 2A). Further syn−anti axial−equatorial carboxylate bridging between Cu(1) atoms in different planes results in the formation of the crystallographic 3D network (Figure 2B).

The Cu(2) atom has a pentacoordinate geometry which is intermediate between square-pyramidal and trigonal-bipyramidal. The angles at Cu(2) range from the ligand bite angle of 81.7(2)° [N(2)−Cu(2)−O(3)] to the trans angle of 165.8(2)° [N(2)−Cu(2)−O(4^{ii})] (Table 2). A pyrazole nitrogen N(2) and a carboxylate oxygen O(3) from one carboxylate group on the dcp^{3-} ligand occupy two coordination sites on Cu(2) [Cu(2)−N(2), 1.973(5) Å; Cu(2)−O(3), 2.042(5) Å]. Two further positions are occupied by water molecules [Cu(2)−O(5), 1.956(6) Å; Cu(2)−O(6), 2.230(6) Å]. The coordination sphere is completed by coordination of a carboxylate oxygen, O(4^{ii}) from the adjacent trimer at $\{-x + 2, y + {}^1/_2, -z + {}^1/_2\}$ to Cu(2) [Cu(2)−O(4^{ii}), 1.955(4) Å]. These essentially planar bridges constitute the backbone of a two-dimensional network of trimers. Irrespective of which five-coordinate geometry is adopted, it is important to note that the Cu(2)−O(4^{ii}) bond and that of Cu(2)−O(3) have relatively short bond lengths. Hence, these can be considered as equatorial bonds. Therefore, the carboxylate bridging mode between Cu(2) atoms of neighboring trimers in the sheet is essentially syn−anti equatorial−equatorial. This is only one of many carboxylate bridging conformations which can be adopted in complexes. It has previously been reported that for Cu(II) complexes triatomic syn−syn and anti−anti carboxylate conformations mediate large and weak to medium antiferromagnetic interactions, respectively, whereas syn−anti and monatomic conformations exhibit weak magnetic exchange interactions.[25]

In the case of the central six-coordinate copper in the trimeric unit, Cu(1), the geometry seen is distorted octahedral. A pyrazole nitrogen atom [Cu(1)−N(1), 1.978(5) Å], and a carboxylate oxygen [Cu(1)−O(1), 1.960(5) Å], on each dcp^{3-} ligand form the distorted equatorial plane around Cu(1) with a chelating angle O(1)−Cu(1)−N(1) of only 82.6(2)°. The remaining axial coordination sites (related by the inversion center) are occupied by carboxylate oxygen atoms [Cu(1)−O(2v), 2.673(6) Å], of dcp^{3-} ligands in equivalent trimeric units in adjacent sheets. Bond angles subtended by these apical oxygen atoms and the equatorial plane range from 86.3(2)° [N(1)−Cu(1)−O(2v)] to 100.9(2)° [O(1)−Cu(1)−O(2v)]. The distortion from octahedral geometry of the Cu(1) site is a result of ligand constraints and the Jahn−Teller effect, the latter being responsible for the elongated axial bonds. This Cu(1) coordination sphere leads to a three-dimensional structure where each trimer in the sheet is in effect linked via carboxylate bridges (O(1)−C(4)−O(2)) to four equivalent trimeric units in adjacent planes (see Figure 2). This syn−anti axial−equatorial carboxylate bridging between planes completes the extended structure seen for **1**.

The dcp^{3-} ligand conformation is not strictly planar. Deviation from the mean plane defined by the pyrazole ring is seen for both carboxylate groups with values ranging from 0.093 to 0.379 Å. The largest deviation is observed for O(2), 0.223(17) Å, and O(3), 0.379(18) Å. The atoms in the pyrazole ring deviate from the mean plane by less than 0.006 Å. The dihedral angle between the two carboxylate mean planes is 15.2(3)°. It can be seen that the ligand bite angle at the two different copper centers Cu(1) and Cu(2) is similar, 82.6(2)° and 81.7(2)°, respectively. This implies that H$_3$dcp is a fairly rigid ligand and retains its integrity on metal chelation. However, the carboxylate groups are twisted out of the plane of the pyrazole ring as a result of the coordination of O(2) and O(3) to their respective coppers. All bond lengths and angles are consistent with those found in comparable structures.[13,26,27]

It is noteworthy that in order to achieve a three-dimensional coordination network, each possible coordination site on the dcp^{3-} ligand is utilized, i.e., its four carboxylate

(25) Colacio, E.; Ghazi, M.; Kivekäs, R.; Moreno, J. M. *Inorg. Chem*. **2000**, *39*, 2882−2890.
(26) Bayon, J. C.; Esteban, P.; Net, G.; Rasmussen, P. G.; Baker, K. N.; Hahn, C. W.; Gumz, M. M. *Inorg. Chem*. **1991**, *30*, 2572−2574.
(27) Bayon, J. C.; Net, G.; Esteban, P.; Rasmussen, P. G.; Bergstrom, D. F. *Inorg. Chem.* **1991**, *30*, 4771−4777.

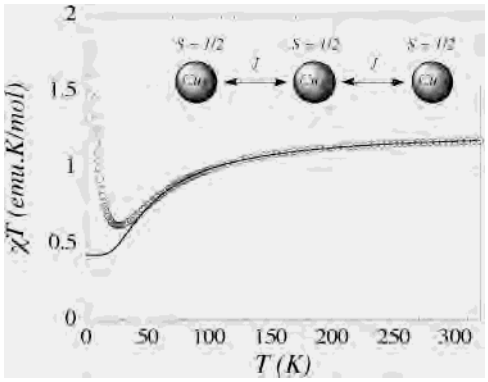

Figure 3. Temperature dependence of χT (where $\chi = M/H$) at 1000 Oe measured on a polycrystalline sample of **1**. Solid lines correspond to the best fits obtained with the $S = {}^1/_2$ trimer model (see text). Inset: scheme of the spin topology in **1**.

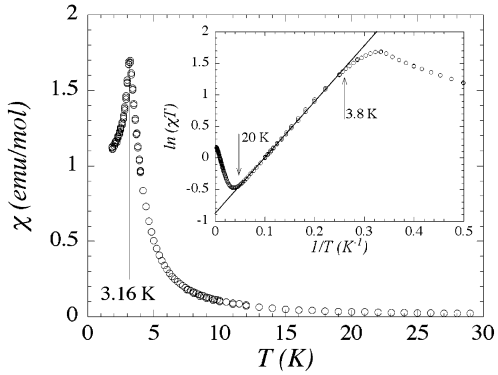

Figure 4. Temperature dependence below 30 K of the magnetic susceptibility χ at 100 Oe measured on a polycrystalline sample of **1**. Inset: $\ln(\chi T)$ versus $1/T$ plot. The solid line indicates the fitting of the experimental data to the 2D Heisenberg model of $S = {}^1/_2$ spins between 20 and 3.8 K.

oxygens and two pyrazole nitrogens, to link the Cu(II) ions. This results in a very dense packing with a density of 2.54 g·cm^{-3}, as has been previously observed for some compounds made using hydrothermal synthesis. The fact that the spin carriers are more densely packed than in compounds prepared under ambient conditions should also allow for greater degrees of magnetic interaction.

Magnetic Properties. The thermal dependence of the χT product per trimer unit, $Cu_3(dcp)_2(H_2O)_4$, is given in Figure 3. At room temperature, the χT value is 1.18 emu·K/mol which is in good agreement with the expected value of three independent Cu(II) $S = {}^1/_2$ species with a g factor of 2.05. This value was confirmed by EPR measurements exhibiting a single resonance line at an average g of 2.08(1).

Upon cooling, the χT value decreases to a minimum of 0.62 emu·K/mol at ca. 27 K. Below this temperature, χT increases to reach a maximum of 5.4 emu·K/mol at ca. 3 K and finally decreases again to 3 emu·K/mol at 1.83 K. A complementary view of these results is given in Figure 4 which shows that the susceptibility exhibits a sharp maximum at 3.16 K.

This complicated behavior can be understood in terms of three stages. First, the high temperature region between 300 and 50 K reveals the presence of dominant antiferromagnetic interactions between the Cu(II) ions within the trimer unit

Scheme 2. Energy Levels of the Isolated Trimer Model[a]

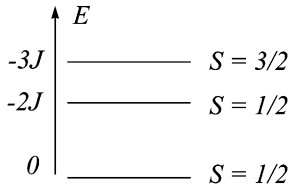

[a] The degeneracies are 2 (for $E = 0$ and $E = -2J$) and 4 (for $E = -3J$).

coupled through the pyrazole nitrogen atoms. This bridging mode is well-known to lead to significant antiferromagnetic coupling.[18,25] To model the high temperature behavior of the magnetic susceptibility, we used as a first approach a simple linear trimer model as shown in the inset of Figure 3. In keeping with this structural motif, the Heisenberg Hamiltonian can be written as follows:

$$\mathbf{H} = -2J\{\mathbf{S}_1\cdot\mathbf{S}_2 + \mathbf{S}_1\cdot\mathbf{S'}_2\} + g\mu_B S_{Tz} H_z \qquad (1)$$

where J is the exchange interaction between adjacent Cu(II) ions in the trimer, $\boldsymbol{S}_i$ the spin operator for each $S = {}^1/_2$ Cu(II), $\mathbf{S}_T$ the total spin operator of the trimer with $\mathbf{S}_T = \mathbf{S}_1 + \mathbf{S}_2 + \mathbf{S'}_2$, S_{Tz} is the z component of the $\mathbf{S}_T$ operator. The diagonalization of eq 1 leads to three energy levels as shown by Scheme 2.

From this diagram, the magnetic susceptibility in the $\mu_B H/k_B T \ll 1$ approximation is given by eq 2.

$$\chi_{trimer}(T) = \frac{Ng^2\mu_B{}^2}{4k_B T}\left\{\frac{1 + \exp(2J/k_B T) + 10\exp(3J/k_B T)}{1 + \exp(2J/k_B T) + 2\exp(3J/k_B T)}\right\} \qquad (2)$$

This model was able to reproduce the experimental data from 300 to 50 K satisfactorily, and it leads to the following set of parameters: $J/k_B = -32$ K and $g = 2.14$. However, below 50 K, this model is not sufficient and intertrimer interactions need to be considered in order to fit the data. From the structural analysis (vide supra), two types of carboxylate bridges have been identified between the Cu(II) trimers: syn−anti equatorial−equatorial bridges form a 2D square lattice, and syn−anti axial−equatorial bridge Cu(1) atoms in different planes lead to the formation of the 3D network. It is well established that these syn−anti coordination modes induce ferromagnetic exchange of the order of a few kelvins (J_{2D}) in the equatorial−equatorial configuration and antiferromagnetic interactions in the range of few tenths of kelvin (J_{3D}) in the axial−equatorial configuration.[25,28] Therefore, the magnetic properties can be described for the second stage by taking into account only the stronger intertrimer interaction (J_{2D}); in other words, the system can be described as noninteracting 2D planes. Below 20 K, Figure 3 shows that the calculated χT for the noninteracting model of trimers saturates, indicating that each trimer can be considered as an effective $S = {}^1/_2$ spin. As long as the interplane interactions (J_{3D}) are negligible, the ferromagnetic interactions between these spins will be described using a

(28) Murugesu, M.; Clérac, R.; Anson, C. E.; Powell, A. K. *Inorg. Chim. Acta*. **2002**, *337*, 328−336

two-dimensional ferromagnetic Heisenberg model in the square lattice case. The exact magnetic susceptibility of this model is known and diverges as $\exp(\pi J_{2D}/k_B T)$.[29,30] Given as an inset in Figure 4 is the semilogarithmic plot of χT versus $1/T$. In agreement with theory, we obtain a straight line between 3.8 and 20 K which confirms the exponential divergence of the susceptibility and fits eq 3 with $C = 0.42$ emu·K/mol and $J_{2D}/k_B = +2.8$ K.

$$\chi_{2D}(T) = \frac{C}{T}\exp\left(\frac{\pi J_{2D}}{k_B T}\right) \tag{3}$$

This value of C is consistent with the Curie constant expected for an $S = {}^1/_2$ system with a g value ($g = 2.10$) close to the value found previously at high temperature with the isolated trimer model ($g = 2.14$). The resulting ferromagnetic interaction J_{2D} is in the range for expected exchange found for a syn−anti equatorial−equatorial coordination mode.[25,31−37]

In stage three, below 3.8 K, the inset of Figure 4 shows that the experimental susceptibility becomes smaller than the prediction of the two-dimensional Heisenberg model emphasising the relevance of antiferromagnetic interplane interactions (J_{3D}). Moreover, the sharp maximum observed at $T_N = 3.16$ K strongly suggests the occurrence of a magnetic phase transition while the 2D Heisenberg model does not predict any long-range magnetic order at finite temperature.[38] Therefore, the weak antiferromagnetic interplane interactions J_{3D} need to be considered in order to discuss the results below 3.8 K. These interactions can be treated in a mean field approximation to estimate the relation between J_{3D} and T_N. This technique has been extensively used to describe quasi-1D[39] or quasi-2D systems.[40,41] In the present case, the value of the exchange J_{3D} can be estimated from the following relationship:

$$z|J_{3D}| = 2k_B T_N \exp\left(-\frac{\pi J_{2D}}{k_B T_N}\right) \tag{4}$$

With $z = 4$, the number of nearest neighbors for a given magnetic site (trimer) in the adjacent planes (Figure 3), $T_N = 3.16$ K and $J_{2D}/k_B = +2.8$ K, we can deduce that $J_{3D}/k_B \sim -0.1$ K. It is worth noting that this value is in good agreement with expected exchange parameters for a syn−anti equatorial−equatorial carboxylate bridge.[25,31−37]

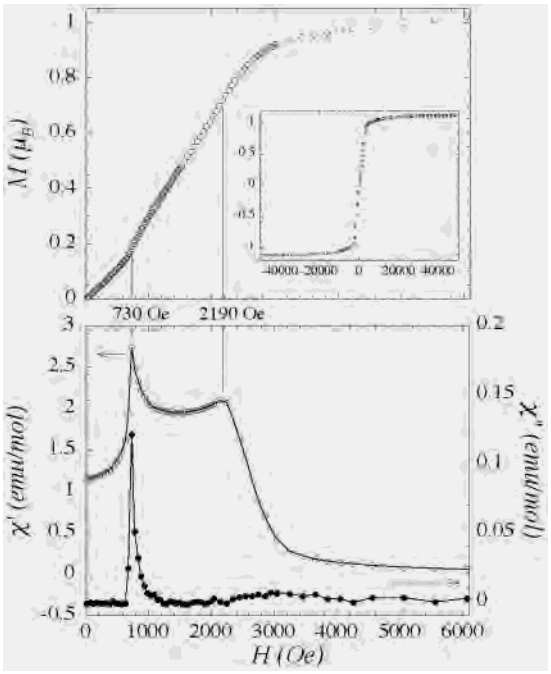

Figure 5. Top: field dependence of the magnetization at 1.8 K and below 6 kOe for **1**. Inset: whole field dependence of the magnetization between −50 and 50 kOe emphasising the absence of a hysteresis effect. Bottom: field dependence (below 6 kOe) of the AC susceptibilities (real and imaginary part, χ' (○) and χ'' (●), respectively) for **1** at 125 Hz and 1.8 K.

The present discussion implies that the magnetic state below T_N is an antiferromagnetic ordered phase resulting from ferromagnetic planes coupled by weak antiferromagnetic interactions. As the interplane interaction (J_{3D}) is weak, it can easily be overcome by an applied magnetic field which is also expected to compete with the magnetic anisotropy. Both effects should contribute to a rich phase diagram in the (T, H) plane. To establish this phase diagram, a more detailed study as function of the applied static field (H) was performed below 3.2 K.

Magnetization (M) and AC susceptibility (in phase $\chi' = dM/dH$[42] and out of phase χ'') have been measured as a function of the magnetic field. At 1.8 K (Figure 5), two anomalies are observed: (i) a kink in the magnetization at $H_{C1} = 730$ Oe which is associated with a sharp maximum in both χ' and χ''; (ii) a maximum of χ' at $H_{C2} = 2190$ Oe corresponding to a deviation from linear field dependence of the magnetization. As shown in the inset of Figure 5 (top), the magnetization saturates at high field to the expected value for $S = {}^1/_2$ (around 1 μ_B per trimer), and no significant hysteresis effect was observed. To describe the magnetic behavior between 1.8 and 3.2 K in more detail, the systematic field dependence of χ' at different temperatures was studied. (Figure 6).

(29) Takahashi, M. *Phys. Rev. Lett.* **1987**, *58* (2), 168−170.
(30) Takahashi, M. *Phys. Rev. B.* **1987**, *36* (7), 3791−3797.
(31) Costa-Filho, A. J.; Nascimento, O. R.; Ghivelder, L.; Calvo,R. *J. Phys. Chem. B* **2001**, *105*, 5039−5047.
(32) Rodrigez-Martin, Y.; Ruiz-Pérez, C.; Sanchiz, J.; Lloret, F.; Julve, M. *Inorg. Chim. Acta* **2001**, *318*, 159−165.
(33) Colacio, E.; Dominguez-Vera, J. M.; Kivekäs, R.; Moreno, J. M.; Romerosa, A.; Ruiz, J. *Inorg. Chim. Acta*. **1993**, *212*, 115−121.
(34) Colacio, E.; Costes, J. P.; Kivekäs, R.; Laurent J. P.; Ruiz, J. *Inorg. Chem.* **1990**, *29*, 4240−4246.
(35) Ruiz-Perez, C.; Sanchiz, J.; Hernandez-Molina, M.; Lloret, F.; Julve, M. *Inorg. Chem.* **2000**, *39*, 1363−1370.
(36) Towle, D. K.; Hoffmann, S. K.; Hatfield, W. E.; Singh, P.; Chaudhuri, P. *Inorg. Chem.* **1988**, *27*, 394−399.
(37) Colacio, E.; Dominguez-Vera, J. M.; Costes, J. P.; Kivekas, R.; Laurent, J. P.; Ruiz, J.; Sundberg, M. *Inorg. Chem.* **1992**, *31*, 774−778.
(38) Mernin, N. D.; Wagner, H. *Phys. Rev. Lett.* **1966**, *17* (22), 1133−1136.
(39) Imry, Y.; Pincus, P.; Scalapino, D. *Phys. Rev. B* **1975**, *12* (5), 1978−1980.
(40) De Groot, H. J. M.; De Jongh, L. J. *Physica B* **1986**, *141*, 1−36.
(41) De Jongh, L. J.; Regnault, L. P.; Rossat-Mignod, J.; Henry, J. Y. *J. Appl. Phys.* **1982**, *53* (11), 7963−7965.

(42) In the present case, the in-phase susceptibility χ' is independent of the frequency below 1000 Hz and therefore can be identified to the derivative of the DC magnetization.

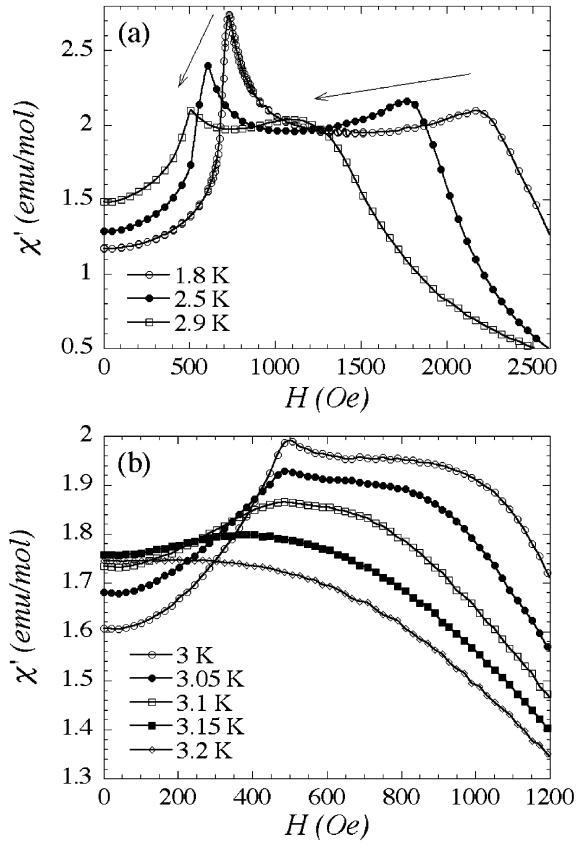

Figure 6. Field dependence of the real part of the AC susceptibility (χ') for **1** at at 125 Hz: (a) below 2.6 kOe and at 1.8, 2.5, and 2.9 K; (b) below 1.2 kOe and between 3 and 3.2 K.

On increasing the temperature from 1.8 to 3 K, both anomalies are still observed and shift toward lower fields (e.g. at 2.9 K, $H_{C1} = 500$ Oe, $H_{C2} = 1120$ Oe). Between 3 and 3.15 K, only one maximum is detectable at a field value which quickly decreases and vanishes between 3.15 and 3.2 K (Figure 6b). These data allow the determination of the transition lines ($H_{C1}(T)$ and $H_{C2}(T)$) in the (T, H) phase diagram. These lines can be better determined from the thermal dependence of χ' (Figure 7) or M at a given field when H_{C1} or H_{C2} are strongly temperature dependent.

Combining all the different types of measurements leads to a well-defined and consistent phase diagram which is shown in Figure 8. The experimental transition lines allow the identification of three different magnetic phases. This type of phase diagram is typical of a weakly anisotropic Heisenberg antiferromagnet.[40] At $H = 0$, the sharp maximum observed at 3.16 K by DC measurements (Figure 4) is confirmed by the AC measurement to be a paramagnetic (P)−antiferromagnetic (AF) phase transition. When the magnetic field is applied, two transition lines corresponding to $H_{C1}(T)$ and $H_{C2}(T)$ are found (Figure 8). The first, which is expected at low field for an anisotropic Heisenberg antiferromagnet,[40] corresponds to the antiferromagnetic (AF)−spin flop (SF) transition. This instability results from the competition between the anisotropy (E_a) and the Zeeman energies[43] and has been modeled to deduce the susceptibility

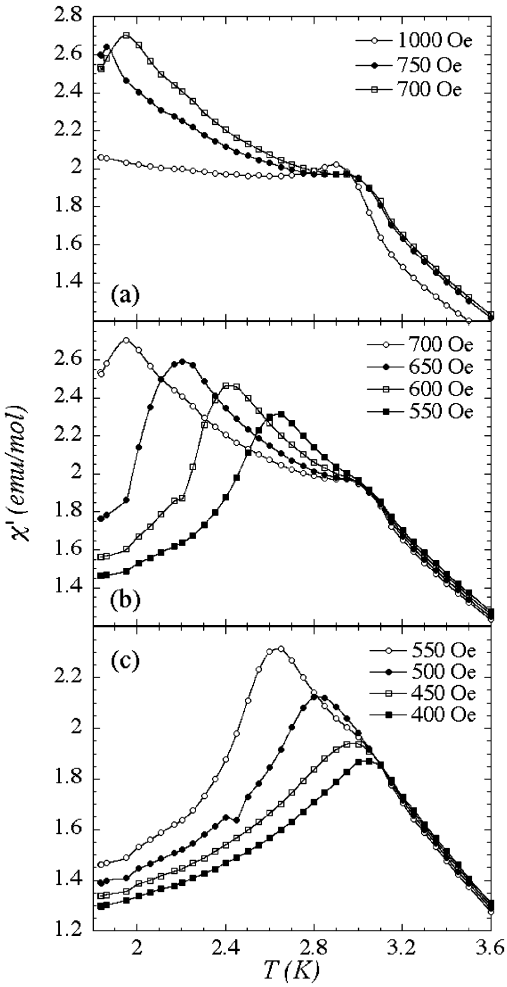

Figure 7. Temperature dependence between 1.8 and 3.6 K of the real part of the AC susceptibility (χ') for **1** at 125 Hz (a) under 1000, 750, and 700 Oe; (b) under 700, 650, 600, and 550 Oe; (c) under 550, 500, 450, and 400 Oe.

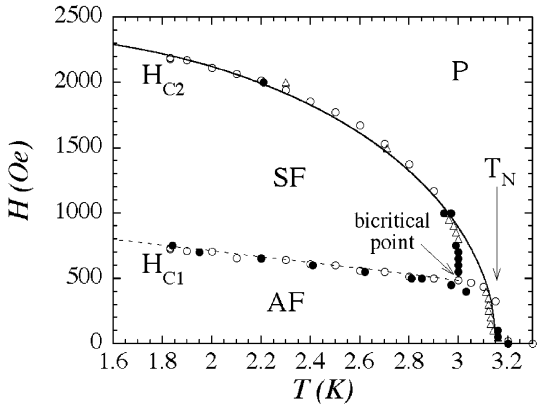

Figure 8. Experimental magnetic phase diagram (T, H) obtained from (●) temperature dependence of the DC susceptibility, (△) temperature dependence of the in-phase AC susceptibility, and (○) field dependence of the in-phase AC susceptibility. Solid (—) and dotted lines (- - -) correspond to the extrapolation models discussed in the text.

on a powder sample.[44] The field dependence of χ' and M shown in Figure 5 reveals the nature of this transition: the susceptibility increases in the AF phase to reach a sharp maximum at the spin flop field (H_{C1}) and saturates in the

(43) Nagamiya, T.; Yosida, K.; Kubo, R. *Adv. Phys.* **1955**, *4*, 1−111.

(44) Uyeda, C.; Date, M. *J. Phys. Soc. Jpn.* **1986**, *55* (8), 2830−2833.

SF phase (below H_{C2}). As expected in this model, H_{C1} is only weakly temperature dependent.[45] The second critical field $H_{C2}(T)$ corresponds to the saturation of the magnetization, i.e., to the SF-saturated paramagnetic (P) phase transition. This saturation occurs when the applied field overcomes the effect of the weak antiferromagnetic interplane coupling (J_{3D}). From theory, $H_{C2}(T)$ is found to be proportional to the temperature dependence of the order parameter, $m(T)$, associated with the magnetic transition.[43] Qualitatively, the experimental result presented in Figure 8 agrees with this prediction.

A quantitative analysis of the effect of the applied field is easier at $T = 0$ K where entropy vanishes. Unfortunately, our lowest experimentally accessible temperature is only of the order of 0.6 T_N. Therefore, the values H_{C1} and H_{C2} at 1.8 K cannot be used and an extrapolation at $T = 0$ K is necessary. The simplest assumption concerning $H_{C1}(T)$ is to extrapolate the linear variation observed between 3 and 1.8 K (dotted line, Figure 8). This extrapolation leads to $H_{C1}(0) = 1150$ Oe, which is most likely an upper limit because a saturation of $H_{C1}(T)$ below 1.8 K cannot be excluded. On the other hand, we estimate $H_{C2}(0)$ to be 2400 Oe using the mean field expression of $m(T)$ for $S = {}^1/_2$: $m = \tanh(m/\tau)$, where τ is the reduced temperature, $\tau = T/T_N$ (continuous line, Figure 8).

At $T = 0$ K, the expressions for $H_{C1}(0)$ and $H_{C2}(0)$ are given by the following equations for $g = 2$:

$$\mu_B H_{C1} = \sqrt{2E_a|J_{3D}|} \tag{5}$$

$$\mu_B H_{C2} = 2|J_{3D}| \tag{6}$$

where E_a is the anisotropy energy in the easy-intermediate plane. With $H_{C2} = 2400$ Oe, we obtain $J_{3D}/k_B = -0.08$ K which is in excellent agreement with the estimation from the T_N (eq 4). Taking the previous value of J_{3D} and $H_{C1}(0) = 1150$ Oe, the estimation of E_a/k_B is 37 mK. This small value may reveal a weak single-ion anisotropy ($D \sim -0.16$ K) but is also consistent with a dipole−dipole anisotropy.[46,47] In any case, the anisotropy is a small contribution to the magnetic energy although it plays a determinant role in the topology of the phase diagram.

To conclude this discussion, let us emphasize the shape of the phase diagram around $T = 3$ K and $H = 485$ Oe which corresponds to a bicritical point.[48] At this point, the effective field-dependent magnetic anisotropy vanishes, and a crossover from Ising-like to *XY*-like critical behavior is expected.[40] Therefore, an enhanced effect of the fluctuations should be observed around this point of the phase diagram. In fact, the signature of these fluctuations is experimentally revealed in Figure 8 as the largest deviation from the mean field behavior (continuous line) is observed around the bicritical point. The ratio (∼0.9) between the temperature of this point and the transition temperature (T_N) is similar to the one observed in other 2D Heisenberg antiferromagnets such as K_2MnF_4,[41] emphasising the universal character of the phase diagram.

Conclusion

We have shown how the hydrothermal synthetic method can be applied to produce a densely packed coordination solid with a rich magnetic behavior. A close analysis of the magnetic phases reveals that the dcp^{3-} ligand acts to couple copper(II) centers in three different ways and with coupling constants orders of magnitude apart in value. These interactions have been estimated and correlated to the structural features and coordination modes of the dcp^{3-} ligand. At temperatures above 50 K, the dominant interaction is relatively strong antiferromagnetic coupling of the copper centers in the trimer units mediated by the pyrazolate bridges of the dcp^{3-} ligand. Below 20 K, this trimer can be modeled as an $S = {}^1/_2$ unit, and weaker ferromagnetic interactions mediated by syn−anti equatorial−equatorial carboxylate bridges linking the trimer units into a square 2D lattice become dominant. Below 3.2 K, we have shown that the material exhibits a three-dimensional antiferromagnetic order with a rich (T, H) phase diagram. This long-range magnetic order is induced by a third antiferromagnetic interaction mediated by syn−anti axial−equatorial carboxylate bridges linking the 2D sheets of the [$Cu_3(dcp)_2(H_2O)_4$] units. Thus, this material demonstrates how it is possible to use the different coordination modes from donors on a single ligand to modulate the degree of magnetic coupling in a system such that several different phases are readily accessible.

These results point the way to making polyfunctional (in terms of magnetic phases) materials where different magnetic states could be accessible at higher temperatures than observed here. An important feature presented by the title compound in the quest to produce polyfunctional magnetic materials is the fact that three types of magnetic coupling dominate in well-separated temperature regions. This characteristic creates a complex magnetic phase diagram and is an important aspect to preserve. This poses the question as to how to increase the critical temperature without losing the rich field-induced phase diagram. An increase of the three parameters J_{2D}, J_{3D}, and the spin state of the repeating unit would raise T_N significantly. On the basis of the theory (eqs 3−6), while all three parameters are important to achieve this goal, the interaction J_{3D} dominates the field behavior (eqs 5 and 6). Therefore, tuning this magnetic exchange would also adjust the field-induced behavior at the same time as raising T_N.

In conclusion, the results we have presented here demonstrate the versatility of carboxylate bridges for transmitting magnetic couplings of different type and intensity. The synthetic challenge lies in designing compounds with the desired carboxylate bridging modes to control the magnetic properties at a microscopic level. This work shows that this approach could be a promising means for obtaining a high-temperature magnetic material with a rich phase diagram which could be used as a polyfunctional device.

(45) Nagamiya, T. *Prog. Theor. Phys.* **1954**, *11* (3), 309−327.
(46) Yosida, K.; Tachiki, M. *Prog. Theor. Phys.* **1957**, *17* (3), 331−359.
(47) Coulon, C.; Laversanne, R.; Amiell, J.; Delhaès, P. *J. Phys. C: Solid State Phys.* **1986**, *19*, L753−L758.
(48) Chaikin, P. M.; Lubensky, T. C. *Principles of condensed matter physics;* Cambridge University Press: London, 1998; pp 172−188.

Acknowledgment. We acknowledge the ESF "Molecular Magnets" program for funding short scientific stays of Rodolphe Clérac and Philippa King. Rodolphe Clérac and Claude Coulon thank also the Conseil Regional d'Aquitaine, and Annie K. Powell, the DFG for financial support.

Supporting Information Available: X-ray crystallographic file, in CIF format. This material is available free of charge via the Internet at http://pubs.acs.org.

IC0261777